JPE 19-2-15

https://doi.org/10.6113/JPE.2019.19.2.497
ISSN(Print): 1598-2092 / ISSN(Online): 2093-4718

# Robust Predictive Speed Control for SPMSM Drives Based on Extended State Observers

Yanping Xu†, Yongle Hou*, and Zehui Li*

†,*Department of Electrical Engineering, Xi'an University of Technology, Xi'an, China

**Abstract**

The predictive speed control (PSC) strategy can realize the simultaneous control of speed and current by using one cost function. As a model-based control method, the performance of the PSC is vulnerable to model mismatches such as load torque disturbances and parameter uncertainties. To solve this problem, this paper presents a robust predictive speed control (RPSC) strategy for surface-mounted permanent magnet synchronous motor (SPMSM) drives. The proposed RPSC uses extended state observers (ESOs) to estimate the lumped disturbances caused by load torque changes and parameter mismatches. The observer-based prediction model is then compensated by using the estimated disturbances. The introduction of ESOs can achieve robustness against predictive model uncertainties. In addition, a modified cost function is designed to further suppress load torque disturbances. The performance of the proposed RPSC scheme has been corroborated by experimental results under the condition of load torque changes and parameter mismatches.

**Key words:** Cost function, Extended state observer (ESO), Model mismatch, Permanent magnet synchronous motor (PMSM), Predictive speed control (PSC)

## I. INTRODUCTION

In many motor applications, including washing machines, industrial robots, electric vehicles and airplanes, permanent magnet synchronous motors (PMSMs) have been widely used, due to their high-power density ratio, simple structure and superior control performance [1]. Field-oriented control [2] and direct torque control [3] have become the standard schemes applied for the speed control of PMSM drives. Recently, due to rapid improvements in microprocessor computational power, model predictive control (MPC) has become extensively employed for motor drives and power electronic converters [4]. According to the system model and state variables at the current moment, MPC can predict future state variables. Then it can obtain the control law by optimizing a cost function. When compared with field-oriented control, MPC has the advantages of high dynamic response, easily achieving multi-objective control and direct handling of system constraints.

The three most widely mentioned MPC methods in motor drives are predictive current control [5], predictive torque control [6] and predictive speed control (PSC) [7]-[10]. The predictive current control and predictive torque control schemes use a PI controller as the outer loop speed controller in most cases. Therefore, the overall dynamic performance of the two strategies is affected by the limited bandwidth of cascaded controllers. The PSC is a cascade-free control scheme that is conducive to improving the system bandwidth. Furthermore, some motor applications such as servo drives and spindle drives require fast speed change. Therefore, the PSC strategy used for speed control is quite attractive.

However, the performance of the PSC is easily affected by model accuracy since the prediction model of PSC is generally derived based on a mathematic model of the system. The system model contains unknown load torque and motor parameters such as permanent magnet flux linkage, stator resistance and stator inductance, and these parameters are variable during motor operation, due to temperature change and the magnetic saturation effect [11]. This means that model parameter uncertainties and the unknown load torque disturbances deteriorate the performance of the PSC. In addition, these problems restrict industrial application of the PSC. Thus, it is necessary to enhance the anti-load disturbance capability and parameter robustness of the PSC.

Manuscript received Jun. 5, 2018; accepted Nov. 23, 2018
Recommended for publication by Associate Editor Young-Doo Yoon.
†Corresponding Author: xuyp@xaut.edu.cn
Tel: +86-029-82312568, Xi'an University of Technology
*Dept. of Electrical Eng., Xi'an University of Technology, China

Many improved methods have been reported for model mismatch problems with the MPC. These methods can be divided into three types. The first type is the embedded integral method. In [12], in order to deal with parameter uncertainties and unmodeled dynamics, the integral terms are added to the prediction model. In [13], a predictive current control strategy based on an embedded integral method is proposed to eliminate the mismatches of rotor flux and stator inductance. However, the embedded integral method affects the dynamic performance of the MPC due to the problem of integral saturation. The second type is the online parameter identification method. The parameter robustness of the MPC is improved by using the least squares identification algorithm in [14]. However, the computational burden of the online parameter identification method is heavy and it is difficult to implement. The third type is the disturbance estimation method. In [15], an offset-free MPC based on a disturbance estimator is used to overcome the mismatch of the predictive model caused by model uncertainty and nonlinearity. The authors of [16] employed a disturbance observer to enhance the prediction accuracy of the continuous-time MPC, and this method achieves good offset-free tracking performance. In [17], a discrete-time disturbance observer is intended to simplify the prediction model and to realize robustness against parameter perturbation. Moreover, the disturbance estimation method does not need the exact disturbance model, and it can be flexibly used to estimate multiple disturbances.

The extended state observer (ESO) is a disturbance estimation method that does not depend on system model accuracy. An appropriate ESO only demands that two parameters be tuned [18]. The ESO can precisely estimate the lumped unknown disturbances including load torque, friction torque, parameter mismatch and unmodeled dynamics [19]. In [20], an ESO is used to substitute for the complex disturbance model for handling model uncertainty. In [21], an ESO is utilized to estimate the load disturbances in direct-drive elevator control systems, and experimental results show the good dynamic performance of the ESO.

In this paper, in order to reduce the adverse effects of load torque disturbances and model parameter uncertainties on the performance of the predictive speed control, the proposed robust predictive speed control (RPSC) strategy uses two ESOs to observe the lumped disturbances. The torque ESO is employed to estimate the electromagnetic torque reference, and the current ESO is adopted to estimate the voltage errors caused by parameter mismatch. The observed state variables and disturbances are then utilized to correct the prediction model. In addition, the electromagnetic torque is regarded as a control objective in the modified cost function to further suppress load torque disturbances.

The rest of this paper is arranged as follows. The PSC strategy is introduced in Section II. Then the proposed robust predictive speed controller is designed in Section III. The proposed RPSC is confirmed by experiments in Section IV. Finally, some conclusions are presented in Section V.

## II. Predictive Speed Control

### A. SPMSM Model

The dynamic model of the SPMSM based on the *dq*-axis rotating synchronously can be derived as follows:

$$\dot{\omega}_e = \frac{P_n T_e}{J} - \frac{P_n T_L}{J} - \frac{B}{J}\omega_e \tag{1}$$

$$T_e = 1.5 P_n \psi_f i_q \tag{2}$$

$$\begin{cases} \dot{i}_d = -\dfrac{R_s}{L_s} i_d + \omega_e i_q + \dfrac{1}{L_s} u_d \\ \dot{i}_q = -\dfrac{R_s}{L_s} i_q - \omega_e i_d + \dfrac{1}{L_s} u_q - \dfrac{\psi_f \omega_e}{L_s} \end{cases} \tag{3}$$

where $\omega_e$ is the electrical rotor angular speed, $T_e$ is the electromagnetic torque, $T_L$ is the load torque that is generally regarded as an unknown external disturbance, $B$ is the friction coefficient, $P_n$ is the number of poles, $J$ is the equivalent rotor inertia constant, $u_d$ is the $d$-axis voltage, $u_q$ is the $q$-axis voltage, $i_d$ is the $d$-axis current, $i_q$ is the $q$-axis current, $R_s$ is the stator resistance, $L_s$ is the stator inductance, and $\psi_f$ is the rotor flux.

However, it is necessary to use a discrete model of SPMSM to predict the system behavior in each of the sampling periods. The forward Euler discretization method [5] is employed to system models (1), (2) and (3).

$$\omega_e(k+1) = \frac{T_s P_n}{J} T_e(k) + (1 - \frac{T_s B}{J})\omega_e(k) - \frac{T_s P_n}{J} T_L(k) \tag{4}$$

$$T_e(k+1) = 1.5 P_n \psi_f i_q(k+1) \tag{5}$$

$$i_d(k+1) = (1 - \frac{T_s R_s}{L_s}) i_d(k) + T_s \omega_e(k) i_q(k) + \frac{T_s}{L_s} u_d(k) \tag{6}$$

$$\begin{aligned} i_q(k+1) = {} & (1 - \frac{T_s R_s}{L_s}) i_q(k) - T_s \omega_e(k) i_d(k) + \frac{T_s}{L_s} u_q(k) \\ & - \frac{T_s \psi_f \omega_e(k)}{L_s} \end{aligned} \tag{7}$$

where $T_s$ is the sample period. In order to control speed without steady-state errors, an internal model of the reference input (i.e., the integral of the speed error [22]) is used to compensate the prediction model. Therefore, the unknown load torque can be eliminated by introducing an internal model to the prediction model (4). Equation (4) is modified as:

$$\omega_e(k+1) = \frac{T_s P_n}{J} T_e(k) + (1 - \frac{T_s B}{J})\omega_e(k) - \xi_e e_\omega(k) \tag{8}$$

$$e_\omega(k) = e_\omega(k-1) + T_s(\omega_e(k) - \omega_e^*(k)) \tag{9}$$

where $\xi_e$ is the integral gain, $e_\omega$ is the integral of the speed errors, and $\omega_e^*$ is the speed reference.

### B. Cost Function Design

According to the output optimal control theory, the electrical rotor angular speed $\omega_e$ and the $d$-axis current $i_d$ are taken as output state variables [9]. The cost function is designed as:

$$g_1 = \lambda_{i1}(i_d^*(k+1) - i_d(k+1))^2 + \lambda_{\omega 1}(\omega_e^*(k+2) - \omega_e(k+2))^2 \tag{10}$$

where $\lambda_{i1}$ and $\lambda_{\omega 1}$ are the weight coefficients of the $d$-axis current error and the speed error, respectively. $i_d^*(k+1)$ and $\omega_e^*(k+2)$ are the future references of the $d$-axis current and speed, respectively. $i_d(k+1)$ and $\omega_e(k+2)$ are the future prediction values of the $d$-axis current and speed, respectively.

For the SPMSM, the maximum torque per ampere control can be achieved by using the control strategy with $i_d$=0. Therefore, this paper sets $i_d^*(k+1)$=0 and uses (6), (7) and (8) as the prediction model. According to the optimization strategies $\partial g_1/\partial u_d(k)$=0 and $\partial g_1/\partial u_q(k)$=0, the control laws can be derived as follows:

$$\begin{aligned} u_{q\_\mathrm{ref}}(k) = {} & \frac{2\lambda_{\omega 1} J L_s}{3P_n^2 T_s^2 \psi_f}(\omega_e^*(k+2) + \xi_e e_\omega(k) \\ & - (1 - \frac{T_s B}{J})\omega_e(k+1)) + \lambda_{\omega 1}(\psi_f \omega_e(k) \\ & + (R_s - \frac{L_s}{T_s})i_q(k) + L_s \omega_e(k) i_d(k)) \end{aligned} \tag{11}$$

$$\begin{aligned} u_{d\_\mathrm{ref}}(k) = {} & \lambda_{i1}(\frac{L_s}{T_s} i_d^*(k+1) + (R_s - \frac{L_s}{T_s})i_d(k) \\ & - L_s \omega_e(k) i_q(k)) \end{aligned} \tag{12}$$

where $u_{d\_\mathrm{ref}}(k)$ is the $d$-axis voltage reference and $u_{q\_\mathrm{ref}}(k)$ is the $q$-axis voltage reference. In order to minimize the cost function $g_1$ by using the control laws (11) and (12), the conditions $\partial^2 g_1/\partial u_{d\_\mathrm{ref}}(k)^2>0$ and $\partial^2 g_1/\partial u_{q\_\mathrm{ref}}(k)^2>0$ must be satisfied. Thus, the weight coefficients should satisfy $\lambda_{i1}>0$ and $\lambda_{\omega 1}>0$.

### C. Current and Voltage Constraints

In order to limit the current in dynamic processes (such as motor start-up and speed changes), the current is predicted again by using the obtained voltage references $u_{d\_\mathrm{ref}}(k)$ and $u_{q\_\mathrm{ref}}(k)$ in (13) and (14), and the predicted state variables are defined as $i_{dp}$ and $i_{qp}$.

$$i_{dp} = (1 - \frac{T_s R_s}{L_s})i_d(k) + T_s \omega_e(k) i_q(k) + \frac{T_s}{L_s} u_{d\_\mathrm{ref}}(k) \tag{13}$$

$$\begin{aligned} i_{qp} = {} & (1 - \frac{T_s R_s}{L_s})i_q(k) - T_s \omega_e(k) i_d(k) + \frac{T_s}{L_s} u_{q\_\mathrm{ref}}(k) \\ & - \frac{T_s \psi_f \omega_e(k)}{L_s} \end{aligned} \tag{14}$$

The maximum current limit is defined as $I_{\max}$. According to the principle of deadbeat control, let $i_q(k+1)=I_{\max}$. Then the new control law can be derived as follows by using (7):

$$\begin{aligned} u_{q\_\mathrm{sat}}(k) = {} & \frac{L_s}{T_s} I_{\max} + (R_s - \frac{L_s}{T_s})i_q(k) \\ & + L_s \omega_e(k) i_d(k) + \psi_f \omega_e(k) \end{aligned} \tag{15}$$

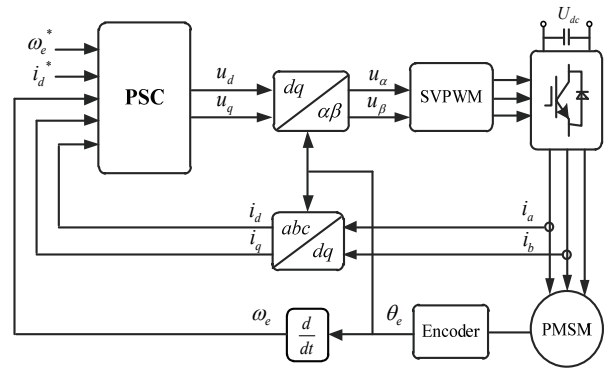


Fig. 1. Schematic block diagram of the SPMSM drive system with the predictive speed control algorithm.

where $u_{q\_\mathrm{sat}}(k)$ is the saturation value of the $q$-axis voltage. When $i_{dp}^2 + i_{qp}^2 \geq I_{\max}^2$, the control laws are switched from (11) and (12) to (12) and (15). Otherwise the controller continues to use (11) and (12) as control laws. Meanwhile, in order to limit the voltage peak while considering the linear modulation region of SVPWM, the maximum voltage amplitude is defined as $|\boldsymbol{u}|_{\max}=U_{dc}/\sqrt{3}$, where $U_{dc}$ is the DC bus voltage. The current constraint method and the overmodulation strategy are shown as follows:

$$|\boldsymbol{u}^*| = \begin{cases} \sqrt{u_{d\_\mathrm{ref}}^2 + u_{q\_\mathrm{sat}}^2}, & i_{dp}^2 + i_{qp}^2 \geq I_{\max}^2 \\ \sqrt{u_{d\_\mathrm{ref}}^2 + u_{q\_\mathrm{ref}}^2}, & i_{dp}^2 + i_{qp}^2 < I_{\max}^2 \end{cases} \tag{16}$$

$$\boldsymbol{u} = \begin{cases} \boldsymbol{u}^*, & |\boldsymbol{u}^*| < |\boldsymbol{u}|_{\max} \\ |\boldsymbol{u}|_{\max} e^{j\theta}, & |\boldsymbol{u}^*| \geq |\boldsymbol{u}|_{\max} \end{cases} \tag{17}$$

where $\boldsymbol{u}$ is the actual voltage, $\boldsymbol{u}^*$ is the reference voltage, and $|\boldsymbol{u}^*|$ and $\theta$ are the magnitude and angle of the reference voltage $\boldsymbol{u}^*$, respectively. Fig. 1 shows the overall scheme of the PSC strategy, where $\theta_e$ is the rotor position.

## III. Robust Predictive Speed Control

The prediction model of PSC is based on the mathematic model of the SPMSM, and the system performance is susceptible to model accuracy. Therefore, model parameter uncertainties and load torque disturbances deteriorate the control system performance. This paper presents a robust predictive speed control (RPSC) strategy to handle the problem of model mismatch. In addition, the proposed RPSC method does not introduce an integral path in the controller to avoid overshoot and windup issues. ESOs are used to estimate the lumped disturbances caused by load torque changes and parameter mismatches. The observer-based prediction model is then derived by using the observed state variables and the lumped disturbances. Furthermore, a modified cost function is designed to further suppress load torque disturbances, and a tuning method of the weight coefficients is also discussed.

### A. Extended State Observers Design

The proposed RPSC uses two ESOs to observe lumped unknown disturbances. System external disturbances are estimated by a torque ESO, and internal disturbances caused by parameter uncertainties are estimated by a current ESO.

At the desired equilibrium point of (1), the mechanical dynamics of the SPMSM can be described as:

$$\dot{\omega}_e^* = \frac{P_n T_e^*}{J} - \frac{P_n T_L}{J} - \frac{B}{J}\omega_e^* \tag{18}$$

where $T_e^*$ is the electromagnetic torque reference. By using (1) to subtract (18), the error model is written as:

$$\dot{\omega}_{\text{err}} = \frac{P_n T_e}{J} - \frac{P_n T_e^*}{J} - \frac{B}{J}\omega_{\text{err}} \tag{19}$$

where $\omega_{\text{err}} = \omega_e - \omega_e^*$.

According to the principle of the discrete-time extended state observer [18], the electromagnetic torque reference $T_e^*$ in (19) is expanded into a new state variable. Therefore, based on the error model (19), the torque ESO is designed as:

$$\begin{cases} \hat{\omega}_{\text{err}}(k+1) = T_s(\frac{P_n}{J}T_e(k) - \frac{P_n}{J}\hat{T}_e^*(k) - \frac{B}{J}\omega_{\text{err}}(k) \\ \qquad + c_1\omega_{\text{err}}(k)) + (1 - c_1 T_s)\hat{\omega}_{\text{err}}(k) \\ \hat{T}_e^*(k+1) = \hat{T}_e^*(k) + \frac{c_2 T_s J}{P_n}(\hat{\omega}_{\text{err}}(k) - \omega_{\text{err}}(k)) \end{cases} \tag{20}$$

where $\hat{\omega}_{\text{err}}(k)$ is the estimated speed error, $\hat{T}_e^*(k)$ is the estimated electromagnetic torque reference, and $c_1$ and $c_2$ are the torque ESO gains. The estimated $\hat{T}_e^*(k)$ is made up of the lumped disturbances caused by load torque, friction torque and mechanical parameter mismatches.

Meanwhile, in the predictive models (6) and (7), the lumped disturbances caused by the $dq$-axis current cross-coupling and electrical parameter (such as $R_s$, $L_s$ and $\psi_f$) mismatches are expanded into new state variables. The new state variables are defined as voltage errors $u_{d\_\text{comp}}(k)$ and $u_{q\_\text{comp}}(k)$. Therefore, based on (6) and (7), the current ESO is designed as:

$$\begin{cases} \hat{i}_d(k+1) = T_s(\frac{1}{L_s}u_{d\_\text{comp}}(k) - \frac{R_s}{L_s}i_d(k) + \omega_e(k)i_q(k) \\ \qquad + \frac{1}{L_s}u_d(k) + c_3 i_d(k)) + (1 - c_3 T_s)\hat{i}_d(k) \\ u_{d\_\text{comp}}(k+1) = u_{d\_\text{comp}}(k) + c_4 T_s L_s(i_d(k) - \hat{i}_d(k)) \end{cases} \tag{21}$$

$$\begin{cases} \hat{i}_q(k+1) = T_s(\frac{1}{L_s}u_{q\_\text{comp}}(k) - \frac{R_s}{L_s}i_q(k) - \omega_e(k)i_d(k) \\ \qquad + \frac{1}{L_s}u_q(k) - \frac{\psi_f\omega_e(k)}{L_s} + c_3 i_q(k)) \\ \qquad + (1 - c_3 T_s)\hat{i}_q(k) \\ u_{q\_\text{comp}}(k+1) = u_{q\_\text{comp}}(k) + c_4 T_s L_s(i_q(k) - \hat{i}_q(k)) \end{cases} \tag{22}$$

where $c_3$ and $c_4$ are the current ESO gains, $\hat{i}_d(k)$ and $\hat{i}_q(k)$ are the estimated $dq$-axis currents, $u_{d\_\text{comp}}(k)$ is the compensation value of the $d$-axis voltage, and $u_{q\_\text{comp}}(k)$ is the compensation value of the $q$-axis voltage.

According to the Hurwitz stability criterion [20], ESOs are stable if $c_1$, $c_2$, $c_3$, $c_4$>0. Taking into account the convergence speed and noise suppression, an ESO parameter selection strategy is presented in [21], where $c_1=2\omega_{c1}$, $c_2=\omega_{c1}^2$, $c_3=2\omega_{c2}$, $c_4=\omega_{c2}^2$, $\omega_{c1}$ and $\omega_{c2}$ are the desired bandwidths of the torque ESO and the current ESO, respectively.

### B. Observer-Based Prediction Model

In this paper, the observer-based prediction model used in the RPSC is corrected in each sampling period by using the torque ESO and the current ESO. Therefore, the prediction errors caused by system disturbances can be compensated in the corrected prediction model.

According to (19), the speed prediction model is modified as (23) by using $\hat{\omega}_{\text{err}}(k)$ and $\hat{T}_e^*(k)$. Based on (6) and (7), $i_d(k)$ and $i_q(k)$ are substituted by the estimated values of $\hat{i}_d(k)$ and $\hat{i}_q(k)$, respectively. $u_d(k)$ and $u_q(k)$ are compensated by the estimated values of $u_{d\_\text{comp}}(k)$ and $u_{q\_\text{comp}}(k)$, respectively. The current prediction model is modified as (24) and (25).

$$\omega_{\text{err}}(k+1) = (1 - \frac{T_s B}{J})\hat{\omega}_{\text{err}}(k) + \frac{T_s P_n}{J}(T_e(k) - \hat{T}_e^*(k)) \tag{23}$$

$$\begin{aligned} i_d(k+1) = {} & (1 - \frac{T_s R_s}{L_s})\hat{i}_d(k) + \frac{T_s}{L_s}(u_d(k) + u_{d\_\text{comp}}(k)) \\ & + T_s\omega_e(k)\hat{i}_q(k) \end{aligned} \tag{24}$$

$$\begin{aligned} i_q(k+1) = {} & (1 - \frac{T_s R_s}{L_s})\hat{i}_q(k) + \frac{T_s}{L_s}(u_q(k) + u_{q\_\text{comp}}(k)) \\ & - T_s\omega_e(k)\hat{i}_d(k) - \frac{T_s\psi_f\omega_e(k)}{L_s} \end{aligned} \tag{25}$$

### C. Modified Cost Function

When compared with PSC, the electromagnetic torque is also regarded as a control objective to suppress load torque disturbances in the proposed RPSC strategy. It is noteworthy that the PSC method adopts a cascade-free control structure. When compared with the traditional cascade control structures, the $q$-axis current reference or the electromagnetic torque reference cannot be obtained directly in the PSC since there is no outer loop speed controller. The electrical time constant is generally much smaller than the mechanical time constant of the motion control system, and the slow dynamics of the electromagnetic torque reference can be directly inferred from (18). This means that the electromagnetic torque reference can be observed, and it is reasonable to assume that the observed electromagnetic torque reference of the adjacent sampling period remains constant (i.e., $\hat{T}_e^*(k+1) \approx \hat{T}_e^*(k)$) when $T_s$ is small enough. Thus, the observed electromagnetic torque reference is used as the future reference of the electromagnetic torque. The cost function (10) is modified as:

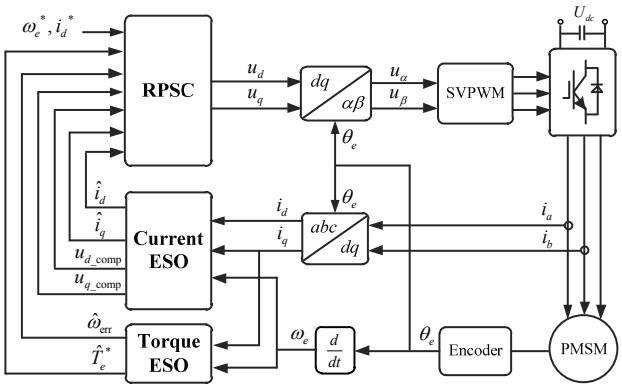


Fig. 2. Schematic block diagram of the SPMSM drive system with the proposed RPSC algorithm.

$$\begin{aligned} g_2 = {} & \lambda_i (i_d^*(k+1) - i_d(k+1))^2 \\ & + \lambda_\omega (\omega_e^*(k+2) - \omega_e(k+2))^2 \\ & + \lambda_T (\hat{T}_e^*(k+1) - T_e(k+1))^2 \end{aligned} \tag{26}$$

where $\lambda_i$, $\lambda_\omega$ and $\lambda_T$ are the weight coefficients of the $d$-axis current error term, the speed error term and the electromagnetic torque error term, respectively. $T_e(k+1)$ is the future prediction value of the electromagnetic torque. According to the optimization strategies $\partial g_2/\partial u_d(k)=0$ and $\partial g_2/\partial u_q(k)=0$, the new control laws can be derived by using the new prediction models (23), (24) and (25) as follows:

$$\begin{aligned} u_{d\_\mathrm{ref2}}(k) = {} & \lambda_i \left(\frac{L_s}{T_s} i_d^*(k+1) + \left(R_s - \frac{L_s}{T_s}\right)\hat{i}_d(k)\right. \\ & \left. - L_s \omega_e(k) \hat{i}_q(k)\right) \end{aligned} \tag{27}$$

$$\begin{aligned} u_{q\_\mathrm{ref2}}(k) = {} & \frac{2\lambda_\omega J L_s}{3P_n^2 T_s^2 \psi_f}\left(\omega_e^*(k+2) - \left(1 - \frac{T_s B}{J}\right)\omega_e(k+1)\right) \\ & + \frac{2(\lambda_\omega + \lambda_T) L_s}{3P_n T_s \psi_f} \hat{T}_e^*(k) - (\lambda_\omega + \lambda_T)\left(\frac{L_s}{T_s}\hat{i}_q(k)\right. \\ & \left. - R_s \hat{i}_q(k) - L_s \omega_e(k) \hat{i}_d(k) - \psi_f \omega_e(k)\right) \end{aligned} \tag{28}$$

where $u_{d\_\mathrm{ref2}}(k)$ and $u_{q\_\mathrm{ref2}}(k)$ are the $d$-axis voltage reference and the $q$-axis voltage reference of the proposed RPSC method, respectively. In order to minimize the cost function $g_2$ using the control laws (27) and (28), the conditions $\partial^2 g_2/\partial u_{d\_\mathrm{ref2}}(k)^2>0$ and $\partial^2 g_2/\partial u_{q\_\mathrm{ref2}}(k)^2>0$ must be satisfied. Therefore, the weight coefficients should satisfy $\lambda_i>0$, $\lambda_T>0$ and $\lambda_\omega>0$.

The overall scheme of the proposed RPSC strategy based on ESOs is shown in Fig. 2. The specific procedure for the proposed RPSC strategy is described as follows.

1) Measure the motor phase current, the DC bus voltage and the rotor position, and calculate the electrical angular speed.
2) Observe the electromagnetic torque reference, the current and the voltage errors according to (20), (21) and (22).
3) Predict the electrical angular speed, the $d$-axis current and the electromagnetic torque according to (5), (23), (24) and(25), and consider the one step delay compensation.

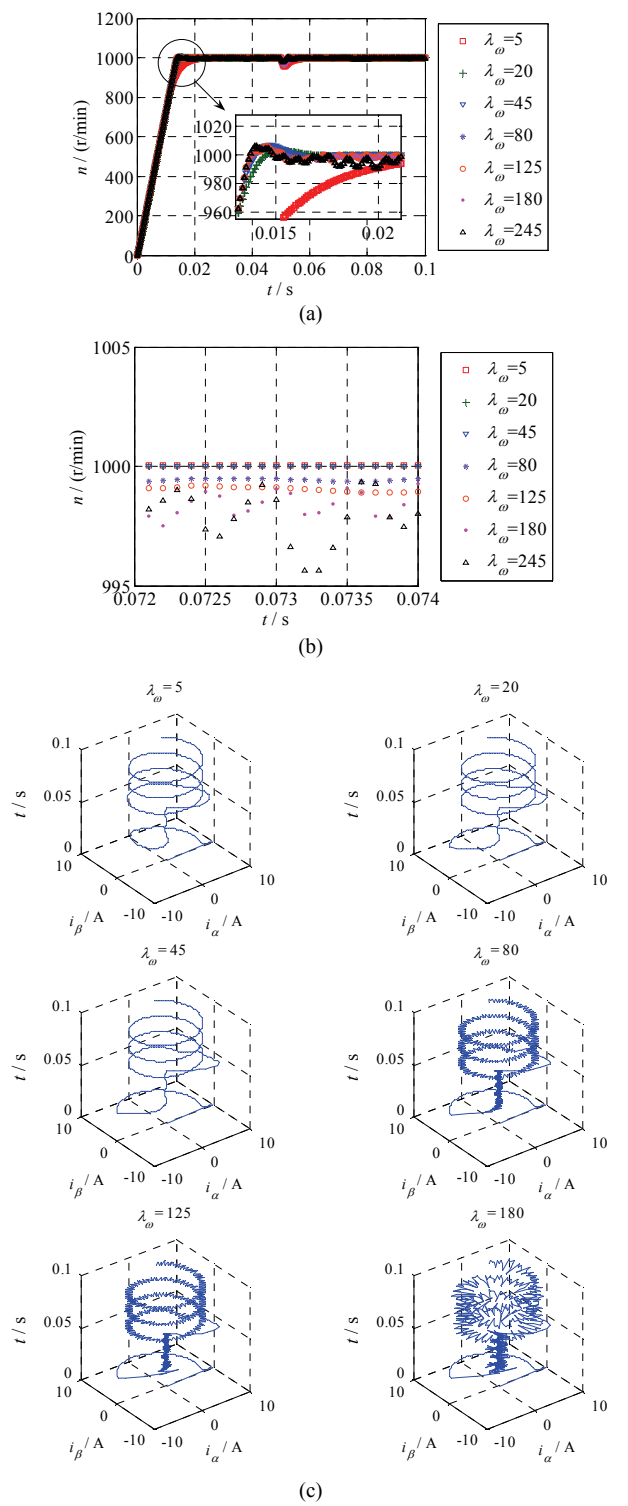


Fig. 3. Simulation results of speed and current responses under different $\lambda_\omega$. (a) Speed responses during motor start-up and torque changes. (b) Speed responses in the steady state. (c) Current responses.

4) Calculate the optimal voltage reference by optimizing the cost function (26).
5) Constrain the motor current and the motor voltage peak according to (15), (16) and (17).

### D. Weight Coefficients Tuning

According to the cost function (26), the performance of the proposed RPSC is closely related to the weight coefficients ($\lambda_i$, $\lambda_\omega$ and $\lambda_T$). In order to ensure both the steady-state performance and the dynamic performance of the RPSC, a tuning method is used to determine the three weight coefficients $\lambda_i$, $\lambda_\omega$ and $\lambda_T$. First, the weight coefficients ($\lambda_i$ and $\lambda_T$) are calculated by using the normalization method. Thus, the weight coefficients ($\lambda_i$ and $\lambda_T$) can be initialized to $\lambda_i=1/I_N$ and $\lambda_T=1/T_N$, where $I_N$ and $T_N$ are the rated current and rated torque of the motor, respectively. Then in order to achieve an improved dynamic performance without distorting the motor current, only the weight coefficient $\lambda_\omega$ needs to be tuned.

The weight coefficient $\lambda_\omega$ is tuned by conducting a sensitivity analysis as shown in Fig. 3. The simulation operating condition is that the speed reference step is from 0 to 1000 r/min, and the rated load is suddenly added at 0.05s. This shows that the speed responses get faster with a larger $\lambda_\omega$ during the transient process in Fig. 3(a). However, Fig. 3(b) shows that the speed steady-state error and speed ripples increase with a larger $\lambda_\omega$. In addition, Fig. 3(c) shows that the current ripples increase with a larger $\lambda_\omega$. Thus, the weight coefficient $\lambda_\omega$ can be determined by considering the steady state performance and dynamic performance of the system.

## IV. Experimental Results

### A. Experimental Setup

The main SPMSM parameters are presented in Table I and the laboratory platform is shown in Fig. 4. It is composed of two 2400W SPMSM motors. One is the prototype motor and the other is the load motor. The experiment is conducted using the Expert3 system of MyWay company. The core controller of the Expert3 system consists of a TMS320C6713 DSP chip and a SPARTAN-XC3S1500 FPGA chip. The C6713DSP, which has powerful computing power and can satisfy the need for verifying various algorithms, is mainly used for core algorithm computations. The FPGA is used for the signal sampling, high-speed I/O and PWM signal generation of the control circuit. Considering the operational precision and DSP computing power, the inverter switching frequency is set to 10kHz. The 2500-line incremental encoder integrated into the motor is used to measure the rotor position. The adjustable parameters of the proposed RPSC are presented in Table II. The weight coefficients of the PSC are $\lambda_{i1}$=0.25 and $\lambda_{\omega 1}$=35.

### B. Performance Comparison of PSC and RPSC

First, the motor parameters used by the controllers are initialized to the rated values in Table I. The experimental results shown in Fig. 5 are the motor start-up and speed change responses of the PSC method and the proposed RPSC method. In order to evaluate the control performances of the two methods, some speed reference steps have been applied to the systems. The first speed reference step is from 0 to 500 r/min, the second step is from 500 to 1000 r/min and the third step is from 1000 to 500 r/min. Fig. 5 shows that the dynamic responses of the electromagnetic torque, speed and current of the proposed RPSC method are similar to those of the PSC method. However, the steady state response of the proposed RPSC method is better than that of the PSC method. Fig. 5(a) shows that the *d*-axis current of the PSC method has steady state errors under different speeds, and that this is caused by the model uncertainty that is not considered in the PSC method. It can be observed that the steady-state error of the *d*-axis current of the proposed RPSC method is almost zero in Fig. 5(c). This confirms that the proposed RPSC method has better steady-state performance than the PSC method.

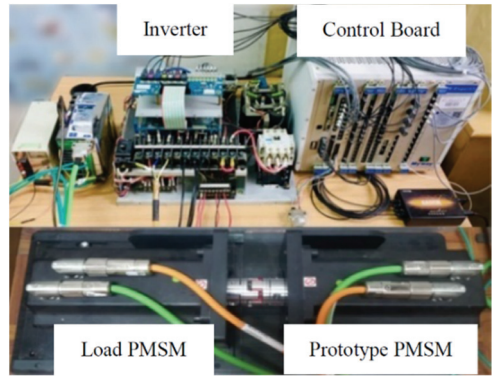


Fig. 4. Photo of the laboratory platform.

TABLE I
MAIN PARAMETERS OF THE SPMSM

| Parameters | Symbols | Rated Values |
|---|---|---|
| Power | $P_N$ | 2400 W |
| Speed | $n_N$ | 2430 r/min |
| Torque | $T_N$ | 9.6 N•m |
| phase current | $I_N$ | 4.4 A |
| stator resistance | $R_s$ | 2.725 Ω |
| Statorinductance | $L_s$ | 21.7 mH |
| inertia constant | $J$ | $1.1\times10^{-3}$ kg•m$^2$ |
| number of pole pairs | $P_n$ | 4 |
| rotor flux | $\psi_f$ | 0.25 Wb |

TABLE II
MAIN PARAMETERS OF THE PROPOSED RPSC ALGORITHM

| Parameters | Symbols | Values |
|---|---|---|
| weight coefficient of speed | $\lambda_\omega$ | 35 |
| weight coefficient of torque | $\lambda_T$ | 0.5 |
| weight coefficient of current | $\lambda_i$ | 0.25 |
| maximum current limit | $I_{max}$ | 10 A |
| maximum voltage limit | $\lvert u\rvert_{\max}$ | 311 V |
| bandwidth of current ESO | $\omega_{c1}$ | 6000 rad/s |
| bandwidth of torque ESO | $\omega_{c2}$ | 500 rad/s |
| DC bus voltage | $U_{dc}$ | 540 V |

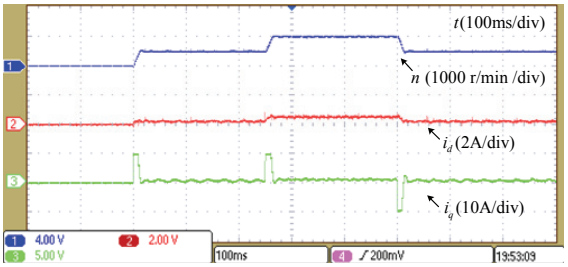


(a)

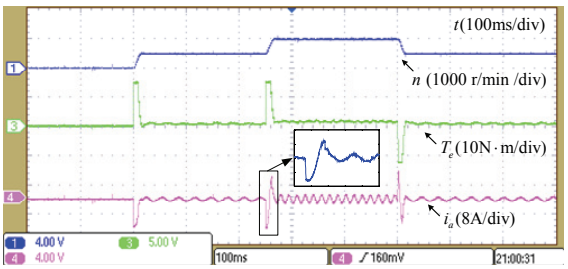


(b)

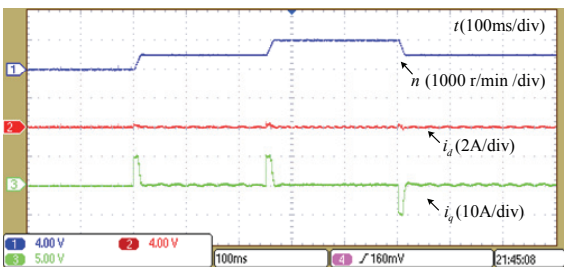


(c)

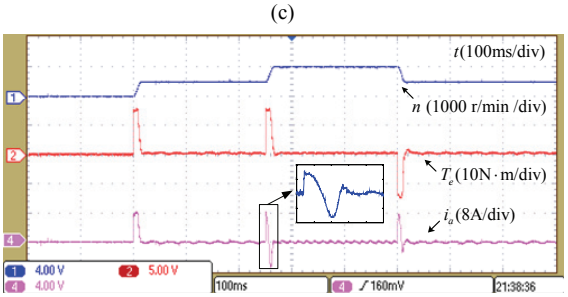


(d)

Fig. 5. Experimental results of motor start-up and speed changes comparisons between: (a) PSC, (b) PSC, (c) RPSC, (d) RPSC.

Fig. 6 shows experimental responses of the PSC method and the proposed RPSC method to the rated load. The experimental operating condition is that the rated load is suddenly added at 0.8 s, and then suddenly removed at 3.15 s. When compared with Fig. 6(a), Fig. 6 (b) shows that the speed of the proposed RPSC method has a shorter recovery time than the PSC method when suddenly adding or removing the rated load. The speed recovery times of the PSC method and the proposed RPSC method are 0.08 s and 0.03 s, respectively. The phase current THD of the PSC method is 4.73% and the phase current THD of the proposed RPSC method is 3.31%, when motor speed is 2000 r/min under full load. The current THD is calculated using experimental data. These results illustrate that the proposed RPSC method has better load disturbance rejection capability than the PSC method. This is due to the use

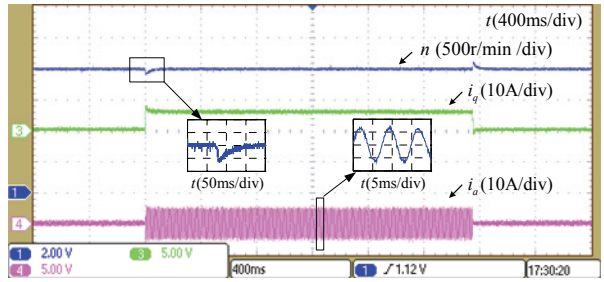


(a)

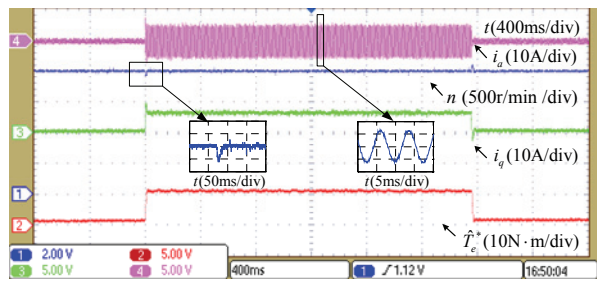


(b)

Fig. 6. Experimental results of load torque changes comparison between: (a) PSC, (b) RPSC.

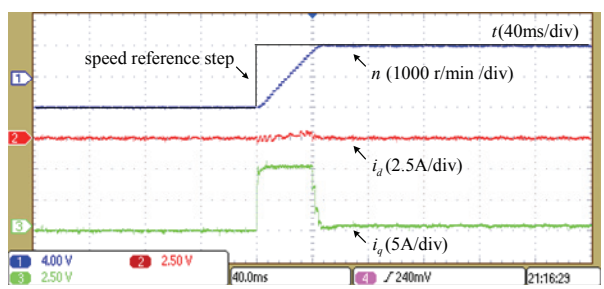


(a)

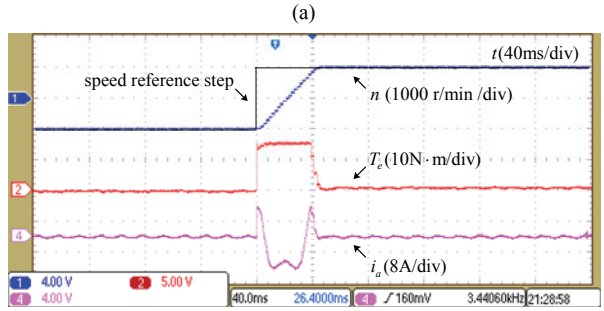


(b)

Fig. 7. Experimental results of the speed reversal of the proposed RPSC method.

of the modified cost function and the observer-based prediction model.

Experimental results of the speed reversal responses of the proposed RPSC method are shown in Fig. 7, the speed reference step applied to the system is from -1000 to 1000 r/min. Fig. 7 shows the good dynamic and steady responses of the speed, current and electromagnetic torque of the proposed RPSC method. Moreover, the *d*-axis current of the proposed RPSC method can remain zero under different speeds, and the phase current and the *q*-axis current both show the desired behavior without exceeding the maximum current limit of 10A.

### C. Parameter Robustness Comparison Between PSC and the Proposed RPSC

In Fig. 8, 9 and 10, the speed reference step is from 0 to 1000 r/min. $|\psi_s|$ is the stator flux amplitude.

In Fig. 8, the robustness of the rotor flux mismatch is compared between the PSC and RPSC. The rotor flux used by the controllers is $2.5\psi_f$, and other motor parameters used by controllers are the rated values. Fig. 8(a) shows that the $q$-axis current of the PSC method is larger than the maximum current limit of 10 A during the transient process. This means that the mismatch of rotor flux deteriorates the dynamic performance of the PSC method. When compared with the PSC method, it can be observed in Fig. 8(c) that the $q$-axis current of the proposed RPSC method is constrained within the maximum current limit when the rotor flux is mismatched. A quantitative comparison of the steady state performance of the two methods under rotor flux mismatch is shown in Table III, where the steady-state errors and the ripples are both calculated using the acquired experimental data. It can be seen that the RPSC method has better dynamic performance and steady state performance than the PSC method under the condition of rotor flux mismatch. These results show that the proposed RPSC method can effectively weaken the adverse effects of rotor flux mismatch on the system performance.

In Fig. 9, the robustness of the stator inductance mismatch is compared between PSC and RPSC. The stator inductance used by the controllers is $2.5L_s$, and the other motor parameters used by controllers are the rated values. In Fig. 9(a) and 9(b), the $d$-axis current, the $q$-axis current, the electromagnetic torque and the stator flux of PSC have severe ripples and the phase current of PSC also has serious distortion, when the stator inductance used by the controller is mismatched. These results show that the PSC method is very sensitive to the stator inductance, and that stator inductance mismatch leads to serious deterioration of the system performance. When compared with the PSC method, Fig. 9(c) and 9(d) show that the ripples of the $d$-axis current, the $q$-axis current, the electromagnetic torque andthe stator flux of RPSC are noticeably smaller and that the phase current of RPSC has less distortion. A quantitative comparison of the steady state performancesof PSC and RPSC under the stator inductance mismatch is given in Table IV. These results indicate that the proposed RPSC method based on ESOs has stronger stator inductance robustness than the PSC method.

In Fig. 10, the robustness of the stator resistance mismatch is compared between PSC and RPSC. It can be seen that the stator resistance used by controllers is $10R_s$, and that the other motor parameters used by controllers are the rated values. Fig. 10(a) and 10(b) show that the $q$-axis current and the phase current of PSC have exceeded the maximum current limit of 10 A during the dynamic process, when the stator resistance is mismatched. However, Fig. 10(c) and 10(d) show that the $q$-axis current and the phase current of RPSC can be constrained within the maximum current limit of 10 A under the condition of stator resistance mismatch. A quantitative comparison of the steady state performance of PSC and RPSC under the stator

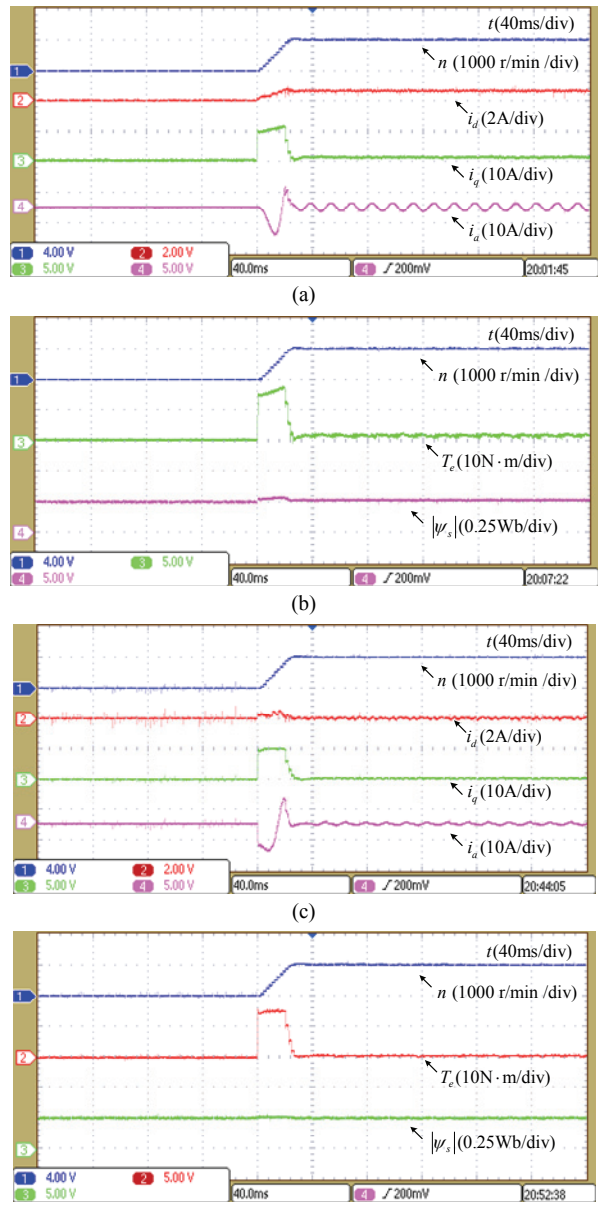


Fig. 8. Experimental results of the rotor flux robustness comparison between PSC and RPSC when the rotor flux is $2.5\psi_f$: (a) PSC. (b) PSC. (c) RPSC. (d) RPSC.

TABLE III
PERFORMANCE COMPARISON BETWEEN PSC AND RPSC UNDER ROTOR FLUX MISMATCH

| Items | PSC | RPSC |
|---|---|---|
| d-axis current ripples | 0.16 A | 0.11 A |
| q-axis current ripples | 0.41 A | 0.14 A |
| electromagnetic torque ripples | 0.31 N•m | 0.18 N•m |
| stator flux ripples | 0.0056 Wb | 0.0052 Wb |
| d-axis current steady state error | 0.57 A | 0.04 A |
| speed steady state error | 23.1 r/min | 7.6 r/min |

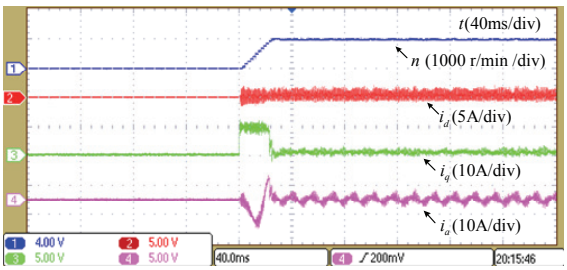


(a)

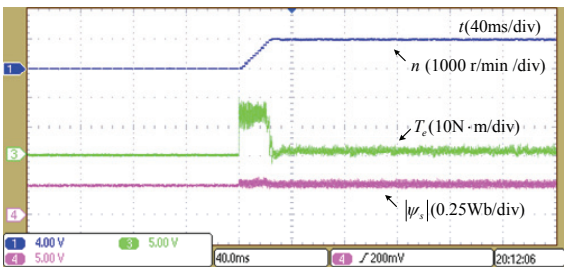


(b)

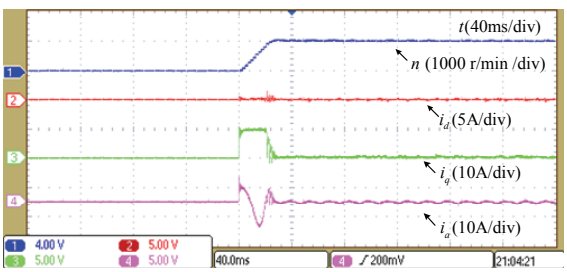


(c)

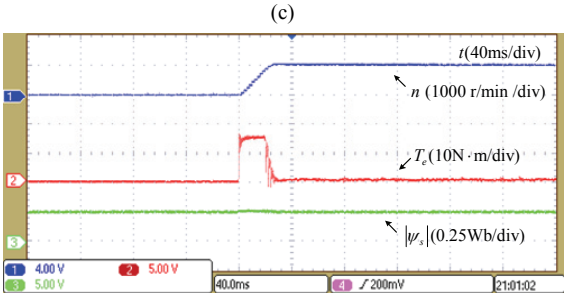


(d)

Fig. 9. Experimental results of the stator inductance robustness comparison between PSC and RPSC when the stator inductance is $2.5L_s$. (a) PSC. (b) PSC. (c) RPSC. (d) RPSC.

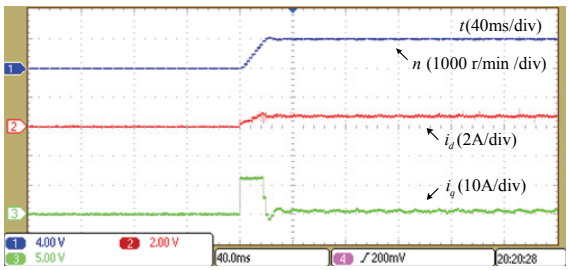


(a)

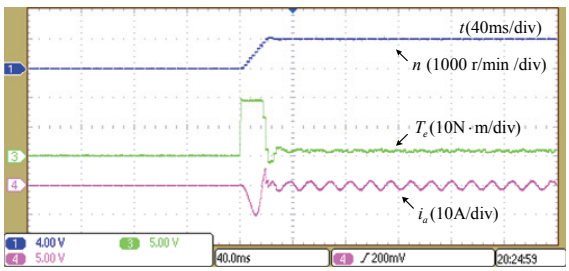


(b)

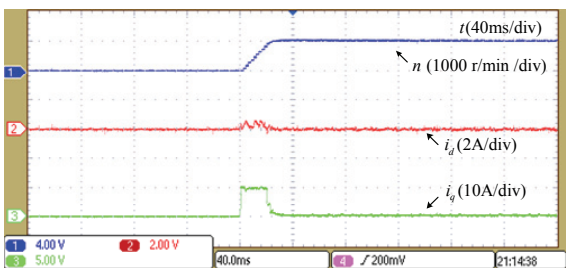


(c)

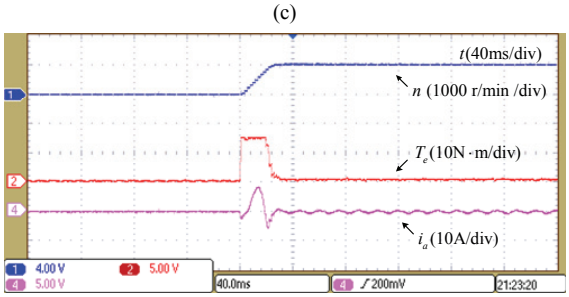


(d)

Fig. 10. Experimental results of the stator resistance robustness comparison between PSC and RPSC when the stator resistance is $10R_s$. (a) PSC. (b) PSC. (c) RPSC. (d) RPSC.

TABLE IV
PERFORMANCE COMPARISON BETWEEN PSC AND RPSC UNDER STATOR INDUCTANCE MISMATCH

| Items | PSC | RPSC |
|---|---|---|
| d-axis current ripples | 1.36 A | 0.14 A |
| q-axis current ripples | 0.59 A | 0.19 A |
| electromagnetic torque ripples | 0.64 N•m | 0.22 N•m |
| stator flux ripples | 0.0129 Wb | 0.0053 Wb |
| d-axis current steady state error | 0.37 A | 0.04 A |
| speed steady state error | 11.7 r/min | 8.5 r/min |

TABLE V
PERFORMANCE COMPARISON BETWEEN PSC AND RPSC UNDER STATOR RESISTANCE MISMATCH

| Items | PSC | RPSC |
|---|---|---|
| d-axis current ripples | 0.12 A | 0.11 A |
| q-axis current ripples | 0.34 A | 0.17 A |
| electromagnetic torque ripples | 0.27 N•m | 0.19 N•m |
| d-axis current steady state error | 0.65 A | 0.07 A |
| speed steady state error | 8.9 r/min | 6.5 r/min |

resistance mismatch is shown in Table V. When compared with the PSC method, these results verify that the RPSC method has better dynamic performance and steady state performance than the PSC method under stator resistance mismatch. This means that the introduction of ESOs can improve robustness against stator resistance mismatch.

Robustness of inertia constant mismatch experimental

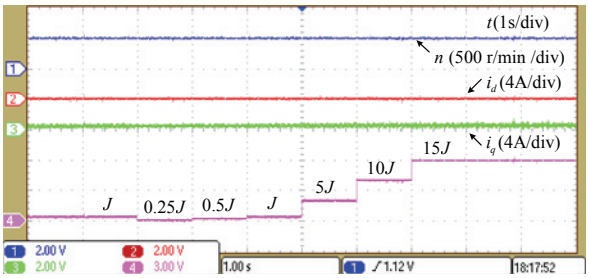


(a)

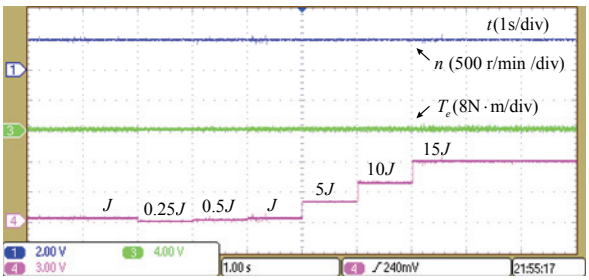


(b)

Fig. 11. Experimental results of the inertia constant robustness of the proposed RPSC method.

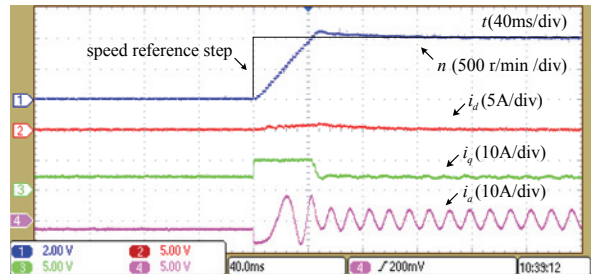


(a)

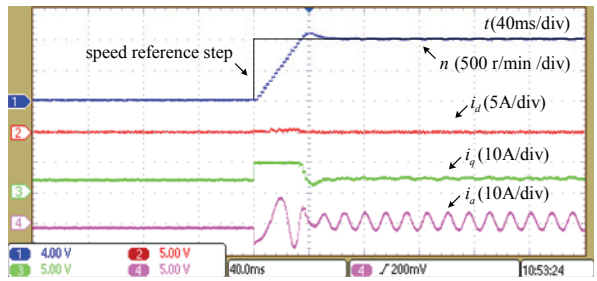


(b)

Fig. 12. Experimental results of the motor starting under load. (a) FOC. (b) RPSC.

results are shown in Fig. 11, and the other motor parameters used by the controllers are the rated values. As Fig. 11(a) and Fig. 11(b) show, the motor runs stably at 500 r/min when the inertia constant used by controller changes suddenly. It can be observed in Fig. 11 that the inertia constant mismatch has little impact on the performance of the proposed RPSC.

### *D. Performance Comparison of Field Oriented Control and the Proposed RPSC*

The following experimental test is carried out to compare the performance of the proposed RPSC with field oriented control (FOC). FOC is a cascade control scheme that contains a speed-loop and a current-loop. The speed-loop uses a PI controller with $K_p$=12 and $K_I$=0.03, which is tuned by using the Ziegler-Nichols method. The current-loop consists of two PI controllers, whose parameters $K_{pi}$ and $K_{ii}$ are designed based on the internal model principle [23], where $K_{pi}=L_s\omega_{c3}$ and $K_{ii}=R_s\omega_{c3}$, and $\omega_{c3}$ is the bandwidth of the current-loop.

In Fig. 12, the experimental operating condition is to start the motor to 1000 r/min under a load torque of 5N·m. Experimental results show that the speed adjustment times of FOC and RPSC are approximately 0.096 s and 0.052 s. When the motor speed is 1000 r/min, with a load torque of 5N·m, the phase current THDs of FOC and RPSC are 5.07% and 4.42%, respectively. When compared with Fig. 12(a), Fig. 12(b) shows that the speed and current of the proposed RPSC have faster responses than the speed and current of FOC. This means that the proposed RPSC has better steady state performance and dynamic performance than FOC.

From the obtained experimental results, when compared with the PSC method, the proposed RPSC method has better dynamic performance when the load torque suddenly changes. The proposed RPSC method has better dynamic performance and steady state performance than the PSC method under the condition of parameter mismatch. Since the proposed RPSC strategy uses state variables estimated by ESOs to correct the prediction model in every sampling period, it reduces the sensitivity of the controller to parameters and decreases the adverse effects of the model mismatch on the control system performance. Furthermore, the proposed RPSC strategy considers the electromagnetic torque as the control target to further suppress load torque disturbance.

## V. CONCLUSIONS

This paper proposes a robust predictive speed control (RPSC) strategy for dealing with the model mismatches caused by load torque changes and parameter uncertainties. The prediction model used by the RPSC strategy is compensated by two extended state observers to enhance algorithm robustness against parameter mismatch without introducing an integral path in the controller. A modified cost function is designed to further suppress the load torque disturbance. When compared with the PSC strategy, experimental results show that the proposed RPSC strategy has better load disturbance rejection capability and stronger parameter robustness. Future works will discuss and reduce the adverse effects of cogging torque, dead-time effects and encoder quantization under the proposed control strategy.

## REFERENCES

[1] I. Petrov, M. Niemelä, P. Ponomarev and J. Pyrhönen, “Rotor surface ferrite permanent magnets in electrical machines: Advantages and limitations,” *IEEE Trans. Ind.*

*Electron.*, Vol. 64, No. 7, pp. 5314-5322, Jul.2017.

[2] D. L. Mon-Nzongo, T. Jin, G. Ekemb and L. Bitjoka, "Decoupling network of field-oriented control in variable-frequency drives," *IEEE Trans. Ind. Electron.*, Vol. 64, No. 7, pp. 5746-5750, Jul.2017.

[3] X. Zhang, K. Wang, and B. Hou, "Low parameter sensitivity deadbeat direct torque control for surface mounted permanent magnet synchronous motors," *J. Power Electron.*, Vol. 17, No. 5, pp. 1211-1222, Sep. 2017.

[4] S. Vazquez, J. Rodriguez, M. Rivera, L. G. Franquelo, and M. Norambuena, "Model predictive control for power converters and drives: advances and trends," *IEEE Trans. Ind. Electron.*, Vol. 64, No. 2, pp. 935-947, Feb. 2017.

[5] B. Wang, Z. Dong, Y. Yu, G. Wang, and D. Xu, "Static-errorless deadbeat predictive current control using second-order sliding-mode disturbance observer for induction machine drives," *IEEE Trans. Power Electron.*, Vol. 33, No. 3, pp. 2395-2403, Mar. 2018.

[6] W. Song, S. Le, X. Wu, and Y. Ruan, "An improved model predictive direct torque control for induction machine drives," *J. Power Electron.*, Vol. 17, No. 3, pp. 674-685, May 2017.

[7] M. Preindl and S. Bolognani, "Model predictive direct speed control with finite control set of PMSM drive systems," *IEEE Trans. Power Electron.*, Vol. 28, No. 2, pp. 1007-1015, Feb. 2013.

[8] E. Fuentes, D. Kalise, J. Rodríguez, and R. M. Kennel, "Cascade-free predictive speed control for electrical drives," *IEEE Trans. Ind. Electron.*, Vol. 61, No. 5, pp. 2176-2184, May 2014.

[9] F. Mwasilu, H. T. Nguyen, H. H. Choi, and J. W. Jung, "Finite set model predictive control of interior pm synchronous motor drives with an external disturbance rejection technique," *IEEE/ASME Trans. Mechatron.,* Vol. 22, No. 2, pp. 762-773, Apr. 2017.

[10] P. Kakosimos and H. Abu-Rub, "Predictive speed control with short prediction horizon for permanent magnet synchronous motor drives," *IEEE Trans. Power Electron.*, Vol. 33, No. 3, pp. 2740-2750, Mar. 2018.

[11] J. Yang, W. H. Chen, S. Li, L. Guo, and Y. Yan, "Disturbance/uncertainty estimation and attenuation techniques in PMSM drives - A survey," *IEEE Trans. Ind. Electron.*, Vol. 64, No. 4, pp. 3273-3285, Apr. 2017.

[12] T. Türker, U. Buyukkeles, and A. F. Bakan, "A robust predictive current controller for PMSM drives," *IEEE Trans. Ind. Electron.*, Vol. 63, No. 6, pp. 3906-3914, Jun. 2016.

[13] Y. Li, S. Wang, H. Ji, J. Shi, and S. Huang, "Model parameter correction algorithm for predictive current control of SMPMSM," *J. Power Electron.*, Vol. 16, No. 3, pp. 1004-1011, May 2016.

[14] J. Sawma, F. Khatounian, E. Monmasson, L. Idkhajine, and R. Ghosn, "Analysis of the impact of online identification on model predictive current control applied to permanent magnet synchronous motors," *IET Electr. Power Appl.*, Vol. 11, No. 5, pp. 864-873, May 2017.

[15] G. Wang, J. Qi, J. Xu, X. Zhang, and D. Xu, "Antirollback control for gearless elevator traction machines adopting offset-free model predictive control strategy," *IEEE Trans. Ind. Electron.*, Vol. 62, No. 10, pp. 6194-6203, Oct. 2015.

[16] J. Yang, W. X. Zheng, S. Li, B. Wu, and M. Cheng, "Design of a prediction-accuracy-enhanced continuous-time MPC for disturbed systems via a disturbance observer," *IEEE Trans. Ind. Electron.*, Vol. 62, No. 9, pp. 5807-5816, Sep. 2015.

[17] H. T. Nguyen and J. Jung, "Disturbance-rejection-based model predictive control: Flexible-mode design with a modulator for three-phase inverters," *IEEE Trans. Ind. Electron.*, Vol. 65, No. 4, pp. 2893-2903, Apr. 2018.

[18] X. Li and S. Li, "Speed control for a PMSM servo system using model reference adaptive control and an extended state observer," *J. Power Electron.*, Vol. 14, No. 3, pp. 549-563, May 2014.

[19] W. H. Chen, J. Yang, L. Guo, and S. Li, "Disturbance-observer-based control and related methods - An overview," *IEEE Trans. Ind. Electron.*, Vol. 63, No. 2, pp. 1083-1095, Feb. 2016.

[20] F. Alonge, M. Cirrincione, F. D'Ippolito, M. Pucci, and A. Sferlazza, "Robust active disturbance rejection control of induction motor systems based on additional sliding-mode component," *IEEE Trans. Ind. Electron.*, Vol. 64, No. 7, pp. 5608-5621, Jul. 2017.

[21] G. Wang, Y. Wang, J. Xu, N. Zhao, and D. Xu, "Weight-transducerless rollback mitigation adopting enhanced MPC with extended state observer for direct-drive elevators," *IEEE Trans. Power Electron.*, Vol. 31, No. 6, pp. 4440-4451, Jun. 2016.

[22] T. Tarczewski and L. M. Grzesiak, "Constrained state feedback speed control of PMSM based on model predictive approach," *IEEE Trans. Ind. Electron.*, Vol. 63, No. 6, pp. 3867-3875, Jun. 2016.

[23] Y. Kwon, S. Kim, and S. Sul, "Voltage feedback current control scheme for improved transient performance of permanent magnet synchronous machine drives," *IEEE Trans. Ind. Electron.*, Vol. 59, No. 9, pp. 3373-3382, Sep. 2012.

**Yanping Xu** was born in Henan Province, China, in 1977. She received her B.S. degree from the Xi'an University of Technology, Xi'an, China, in 1999; where she received her M.S. and Ph.D. degrees in Power Electronics and Power Drives, in 2002 and 2008, respectively. She is presently working as an Associate Professor in the Department of Electrical Engineering, Xi'an University of Technology. Her current research interests include power electronics, high performance permanent magnet synchronous motor drives and sensorless control technology.

**Yongle Hou** was born in Shanxi Province, China, in 1994. He received his B.S. degree in Electrical Engineering from Shanghai DianJi University, Shanghai, China, in 2016. He is presently working towards his M.S. degree in Electrical Engineering at the Xi'an University of Technology, Xi'an, China. His current research interests include power electronics, high performance permanent magnet synchronous motor drives and model predictive control.

**Zehui Li** was born in Shaanxi Province, China, in 1990. He received his B.S. degree in Electrical Engineering from Yulin University, Yulin, China, in 2015; and his M.S. degree in Power Electronics and Power Drives from the Xi'an University of Technology, Xi'an, China, in 2018. He is presently working as a R&D Engineer in Shenzhen Hopewind Electric Co., Ltd., Shenzhen, China. His current research interests include high performance permanent magnet synchronous motor drives and sensorless control technology.